Cone-beam projection of a deformable volume for motion compensated algebraic reconstruction

Simon Rit and David Sarrut

***Abstract*— The cone-beam tomographic projection and the deformation of a discrete volume are problems that have generally been studied separately. They are combined in some applications such as motion compensated algebraic reconstruction. In this paper, we propose two methods to compute the cone-beam projections of a volume deformed with a known motion. The first method is based on an inverse mapping between the reference 3D volume and the 2D cone-beam projection and the second method on a forward mapping. Both methods were evaluated on a dynamic digital phantom and confronted to another method. The quality of the cone-beam projections was increased by 70% with both methods compared to the projection obtained without including the motion model. The proposed methods yield accurate linear equations, the first step before tomographic reconstruction of the deformable volume with algebraic methods.**

I. Introduction

The cone-beam projection of a 3D discrete volume is an important problem in image processing and more particularly in medical imaging [1]. It is used for example to compute Digitally Reconstructed Radiographies (DRR), to register a 3D volume on measured cone-beam projections, which is called 2D/3D registration, or to yield linear equations for tomographic reconstruction using algebraic methods.

However, the respiratory and cardiac motions between the acquisition time of the volume and of the cone-beam projections is an issue. In particular, they imply artifacts in tomographic imaging such as blur, streaks and bands. Several solutions have been proposed to correct these artifacts [2]. One of the most promising approaches is motion compensated reconstruction which consists in including the motion model in the reconstruction process. It allows to use all the cone-beam projections for the reconstruction of a 3D Computed Tomography (CT) image and should result in an image with a quality comparable to CT images of static objects.

Analytic algorithms have been the first to be adapted to motion compensated reconstruction. They are either exact but limited to some motions [3] or based on heuristics [4]. The latters are more suited to respiratory and cardiac motions but they do not fully correct the artifacts. Algebraic reconstruction may therefore be a better choice. Other past studies integrate the motion in algebraic reconstruction [5], [6] but, to our knowledge, no work evaluate the accuracy of the linear equations before solving them.

In this paper, we propose two methods to model the cone-beam projection of a discrete volume submitted to a known deformation. One is based on an inverse mapping and the other on a forward mapping between the discrete volume and the computed cone-beam projections. We evaluated the results on a dynamic digital phantom of a thorax and compared them with another method.

This work was supported in part by Elekta Oncology Systems

S. Rit is with the LIRIS, Université Lumière Lyon 2, 5 Av. P. Mendès-France, 69676 Bron, France simon.rit@gmail.com

D. Sarrut is with the CREATIS and the Léon Bérard Center, Department of Radiotherapy, 28 rue Laënnec, 69353 Lyon, France david.sarrut@creatis.insa-lyon.fr

II. Preliminaries

A. Discrete model

The imaging system is modeled in the classical way:

$$A\,V = B \tag{1}$$

where V is the 3D image of patient tissue densities which is unknown in image reconstruction problems, and B is the set of cone-beam projections, i.e. 2D images of attenuations. If the patient remains static during the acquisition of the data B, V is constant in time and A is obtained by modeling the cone-beam transformation in a discrete formulation (see II-C.1). If the patient moves during the acquisition, the assumption that V is constant in time is false. To take this motion into account, measured data B are linked to a reference volume V_{ref} corresponding to the patient position at time $t = t_{\mathrm{ref}}$ and (1) becomes $A\,V_{\mathrm{ref}} = B$. In addition to the cone-beam transformation, A comprises then the patient motion between t_{ref} and each acquisition time t of the cone-beam projections (see II-C.2). In this study, we propose different methods to determine A if the patient motion is known.

B. Image warping

A spatial transformation consists in computing a warped image given a source image and a mapping function. There are two ways to compute the target image [7]. Forward mapping consists in going through the pixels of the source image and copying their intensity onto the target image using the mapping function. Most of the mapping functions do not give a pixel-to-pixel correspondence between source and target images and it is necessary to take into account that each source pixel can contribute partly to several target pixels. The cost for the computation of the exact contribution is expensive and simplifications have generally to be made. There is then no guarantee that all intensities of the target pixels are computed and that the sum of the splitting weights of the source contribution is equal to one for each target pixel. These *holes* and *overlaps* require special management.

Inverse mapping consists in going through the pixels of the target image and getting their intensity from the source image using the inverse of the mapping function and an appropriate interpolation scheme. All target pixels are then computed. Meanwhile, if several pixels of the source contribute to one pixel of the target, the computed intensity may not be accurate. Subdivision of the target pixels may be a solution to avoid such problems.

C. Spatial transformations

1) Cone-beam transformation: Cone-beam projections are acquired around the patient using a punctual source of X rays and a two dimensional detector. The measured attenuations can be linked to the linear sum of tissue densities along X rays which is called *cone-beam transformation*. In the static case, A links the discrete grid of attenuation coefficients with the discrete samples of the cone-beam projections using the cone-beam transformation. Two categories of cone-beam projection methods can be distinguished: voxel-driven projection for forward mapping and ray-driven projection for inverse mapping. In [8], De Man et al detailed the advantages and the drawbacks of the two categories of approaches. Voxel-driven projection needs a proper management of the interpolation kernel projection, like *splatting* [9], to avoid high-frequency artifacts, which is not the case for ray-driven approaches.

2) Respiratory motion: The respiration of the patient is an "involuntary" motion that we cannot stop during the acquisition time. Its measurement generally involves non-rigid registration [5], [10] which output can be described by a 4D motion model:

$$\Phi : \mathbb{R}^3 \times \mathbb{R} \mapsto \mathbb{R}^3 \mid y = \Phi(x,t) = \Phi_t(x) \qquad (2)$$

This function maps the 3D position of a physical point $y = \Phi_t(x)$, at any time t, with its 3D position x at the reference time t_{ref}. We supposed that Φ_t is a diffeomorphism which implies that the inverse function $x = \Phi_t^{-1}(y)$ exists. Different parameterizations of Φ exist and we used in this study a set of discrete 3D vector fields, with a displacement vector for each voxel of the reference volume to the volume corresponding to the cone-beam projection.

III. Methods

The projection of the deformable volume involved the composition of the respiratory motion with the cone-beam transformation (Fig. 1). Providing that both transformations were known, we proposed two methods, one based on an inverse mapping and one based on a forward mapping.

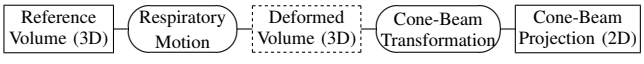

Fig. 1. Link between the reference volume and a cone-beam projection.

A. Inverse mapping

1) Static projection: Among the numerous ray-driven methods to obtain the perspective projection of a volume, we chose the shearwarp algorithm [11]. It is close to Joseph's method [12] because the ray is sampled at each slice of the volume (Fig. 2a) but the perspective is decomposed in two transformations: a shear and a warp (Fig. 2b). The shear pass allows to align the samples of a ray in one major direction of the orthogonal base. An intermediate projection is obtained by summing these samples in the major direction. The cone-beam projection is finally computed with a 2D warp of the intermediate projection using an affine transformation.

2) Motion compensated projection: We want to compute the cone-beam projection of a volume V_t for any time t using the reference volume V_{ref} at a time t_{ref} and the motion model Φ_t between V_{ref} and V_t. We have seen in the previous paragraph that ray-driven methods interpolate V_t intensities along each ray corresponding to each pixel of the cone-beam projection. As V_t is unknown, one can retrieve the intensities from V_{ref} using Φ_t^{-1} whatever the ray-driven method. Fig. 2c illustrates it for the shearwarp factorization. It required two interpolations: the vector field values along the ray, which is implemented with a nearest neighbor interpolation, and the density in V_{ref}, which is implemented with a trilinear interpolation.

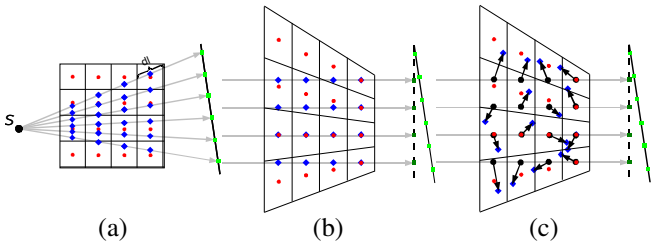

Fig. 2. Inverse mapping methods. (a) Joseph interpolation [12] ; (b) the shearwarp factorization [11], (red circles=sheared volume ; dark green squares=intermediate image) ; (c) inclusion of the vector field in the shearwarp projection with inverse mapping (the arrows represent Φ_t^{-1}).

B. Forward mapping

We propose also a new voxel-driven algorithm based on the shearwarp factorization previously described but adapted to forward mapping. It uses then Φ_t instead of Φ_t^{-1} in the previous method. The algorithm is first described in the static case and then extended to the motion compensated case.

1) Static projection: The original shearwarp method [11] is based on backward mapping to compute the shear. It does not need to store the sheared volume because it directly performs the slice-by-slice sum in the intermediate image. Inverse mapping guarantees indeed that for each pixel of the intermediate image, there is exactly one corresponding intensity value interpolated in each slice of the sheared volume (Fig. 2b). This is not guaranteed with forward mapping and we had to modify the algorithm.

For each voxel x of the source volume, the corresponding position x_s in the sheared volume is computed. This position is between 4 voxels of the corresponding slice of

the sheared volume (Fig. 2b). We store in a sheared volume V_s the intensity of x split in the 4 neighbors with bilinear interpolation. Bilinear weights are added in corresponding voxels of a weigths array V_{sw} with the same dimensions as V_s.

Computed intensities of V_s are normalized with V_{sw} by a voxel-to-voxel division when V_{sw} is not zero to eliminate *overlaps*. When a value in V_{sw} is zero, we have to manage this *hole*. As the contributions of the voxels of the sheared volume to one pixel of the intermediate image are aligned along one direction of the orthogonal base (Fig. 2b), this is done in 1D along this direction. The *holes* are filled with the mean value of its two nearest neighbor which amounts to weight voxels which are not *holes* by one plus half the length (in number of pixels) of its adjacent *holes* (Fig. 3).

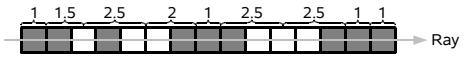

Fig. 3. Weighted sum of voxel intensities (grey) of the sheared volume along the ray when there are *holes* (white).

2) Motion compensated projection: Inclusion of the respiratory motion is now straightforward. For each voxel x_{ref} of the reference volume V_{ref}, we calculate its position $x_t = \Phi_t(x_{\text{ref}})$ in V_t and apply the same algorithm. The only difference is the split of the intensity of x_{ref} in the sheared volume V_s which is this time trilinear because the displacement of a voxel due to the respiratory motion can fall between two slices of V_t. The introduction of more *holes* or *overlaps* due to the forward mapping of the respiratory motion was also corrected with the previously described method.

IV. Experiments

A. Dynamic digital phantom

The digital thorax phantom at the exhale state is a simplified version of the Forbild phantom (Fig. 4). A spherical tumor having a diameter of 3 cm is positioned in the lower part of the right lung. An analytical transformation is applied to this phantom to obtain the inhale state. This transformation is composed of translations and changes of volume of the different geometric parts of the phantom. Intermediate states between inhale and exhale were deduced linearly with a respiratory signal between 0 and 1.

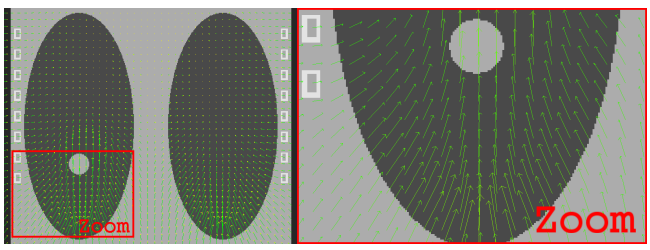

Fig. 4. Coronal slice of the digital phantom at the inhale state (reference), with the computed motion vector field Φ_{1-0} between inhale and exhale states.

B. Respiratory signal

A simulated acquisition of the dynamic phantom was generated with a synthetic respiratory signal $s : \mathbb{R} \mapsto \mathbb{R}$ based on the asymmetric sinusoidal model $s = s_0 + b\cos^{2n}(\pi t/\tau)$ with $n = 2$, $\tau = 4$ s, $s_0 = 0$ and $b = 1$ [13]. The sampling period was set to 0.18 seconds and 640 analytical projections were computed regularly along a circular source trajectory using the open-source software *Take* to simulate the acquisition of a Synergy system™(Elekta Oncology Systems Ltd., Crawley, West Sussex, UK).

C. 4D motion model

End-inhale was chosen as the reference volume V_{ref}. A dense vector field representing the deformation Φ_{1-0} between end-inhale and end-exhale was computed using an optical flow algorithm with a Gaussian regularization [14] (Fig. 4). Φ_{1-0} was evaluated by computing the image of the absolute difference between the end-inhale image (V_{ref}) and the end-exhale image warped with Φ_{1-0}. As intermediate states between end-inhale and end-exhale have been computed linearly, Φ_t was obtained by weighting Φ_{1-0} with $1 - s(t)$ where s is the respiratory signal and t the time of acquisition of the cone-beam projection. We have $\nabla\Phi_t(x) = 1\ \forall x$ because the changes of the voxel densities due to their volume variations were not simulated. This approximation allows to compute analytically the set of cone-beam projections used as reference.

D. Inverse of the respiratory motion

Inverse mapping required the computation of the inverse of the discrete vector field Φ_t^{-1}. It could have been done during the registration process itself. In this study, we chose to inverse Φ_t *a posteriori* with a numerical method, a problem that has been addressed in other works. Our method was divided in three steps. In the first step, we inversed Φ_t in a forward manner: for each vector v of Φ_t, we attributed $-v$ to the vector of Φ_t^{-1} pointed by v. In the second step, the vectors of Φ_t^{-1} which had not been computed in the first step were interpolated with the nearest neighbors. In the last step, each vector of Φ_t^{-1} was adjusted by minimizing in a given neighborhood the L2 norm of the vectors of $\Phi_t \circ \Phi_t^{-1}$. We discretized the respiratory motion in 20 different respiratory positions, which is a relevant approximation regarding the maximum displacement between end-inhale and end-exhale positions which is equal to 30 mm. The 20 inverse vector fields were evaluated by computing the mean norm of the vectors of $\Phi_t \circ \Phi_t^{-1}$ for all points x of the reference image.

E. Projections evaluation

We used V_{ref}, Φ_t and Φ_t^{-1} to compute the projections P_θ with our 2 methods. The results were evaluated quantitatively with the projections P_θ^{ref} computed analytically, using the Signal-to-Noise Ratio (SNR).

Our results were compared to the projection without motion compensation using the basic shearwarp algorithm and to the projection with an existing method proposed by Blondel et al [5]. This method simplifies the problem

by supposing that each voxel of the volume contributes to exactly one pixel of the cone-beam projection and allows a faster computation of the projections. We implemented it as they suggested with a bilinear split based on the distance to the four neighboring pixel centers of the cone-beam projection. We call the method *voxel driven projection with a bilinear split* (VDPBS).

V. Results

A. Respiratory motion

The mean intensity of the error image between the two extrema decreased from 0.076 ± 0.252 g.cm^{-3} without motion compensation to 0.008 ± 0.051 g.cm^{-3} with motion compensation. Remaining errors were located at the borders of the geometric parts. The mean error of the 20 inverse vector fields was less than 0.10 ± 0.05 mm.

B. Projections

The minimum/mean SNR was 14.0/25.5 dB without motion compensation, 37.6/43.4 dB for inverse mapping, 37.2/43.5 dB for forward mapping and 11.7/16.8 dB for VDPBS. We plotted the SNR of each computed cone-beam projection in function of the angle of acquisition θ in Fig. 5. In all cases, the quality of the cone-beam projection decreased when the respiratory motion was large, i.e. for low values of the respiratory signal. The two proposed methods performed almost equally well.

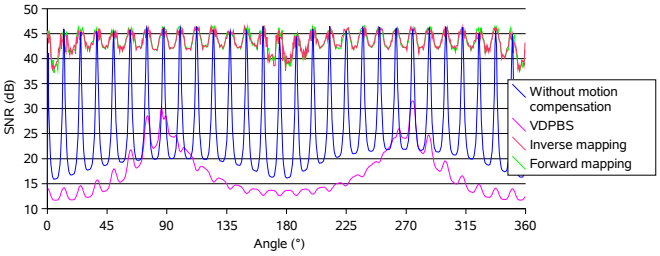

Fig. 5. SNR of the computed projections without motion compensation, with the VDPBS method and with the two proposed methods. The reference is the cone-beam projection computed analytically.

VI. Discussion and Conclusion

The two proposed methods gave similar results in terms of signal quality on the phantom data (Fig. 5). We improved the mean of the SNR from 25 dB if the motion was not taken into account to 43 dB with our two methods. VDPBS method lead to poorer results because the methods does not use an optimal modeling of the transformations, particularly the cone-beam projection. The motion was visually compensated but their results may not be sufficient for thorax imaging depending of the use of the results. However, it was used by Blondel et al [5] to reconstruct images of coronary arteries and they obtain in this case good results and the higher contrast may explain then the robustness to projection approximations.

The computation time was less a preoccupation in this work than the quality of the results. If one excludes the time for the disk inputs and outputs, the forward mapping takes slightly more time (+1%) and memory (+10%) due to the management of the *holes* in the sheared volume. In comparison, Blondel et al method takes much less time (-59%) and memory (-63%), which could be an important criterion for other applications.

Depending on the method used to estimate the motion, one can have Φ_t or/and Φ_t^{-1} available. We propose a method to project the reference volume in each case, which potentially avoids to compute the inverse motion.

Such work represents the initial step of motion compensated algebraic reconstruction. In the static case, the quality of the reconstructed CT images directly depends on the projection method and one can expect the same link in the dynamic case. The accuracy level of the motion model may also strongly influence the results. Obtaining it is still an open problem but Zeng et al [10] proposed to extract it using cone-beam data and an a priori reference volume. This 2D+t/3D registration requires to project the deformable volume in the registration process, which could be done with one of the two algorithms proposed in this article.

References

[1] F. Xu and K. Mueller, "A comparative study of popular interpolation and integration methods for use in computed tomography," in *IEEE International Symposium on Biomedical Imaging (ISBI)*, 2006.

[2] S. Bonnet, A. Koenig, S. Roux, P. Hugonnard, R. Guillemaud, and P. Grangeat, "Dynamic X-ray computed tomography," *Proceedings of the IEEE*, vol. 91, no. 10, pp. 1574–1587, 2003.

[3] L. Desbat, S. Roux, and P. Grangeat, "Compensation of some time dependent deformations in tomography," *IEEE Trans Med Imag*, vol. 26, no. 2, pp. 261–269, 2007.

[4] C. Ritchie, C. Crawford, J. Godwin, K. King, and Y. Kim, "Correction of computed tomography motion artifacts using pixel-specific back-projection," *IEEE Trans Med Imag*, vol. 15, no. 3, pp. 333–342, 1996.

[5] C. Blondel, G. Malandain, R. Vaillant, and N. Ayache, "Reconstruction of coronary arteries from a single rotational X-ray projection sequence," *IEEE Trans Med Imag*, vol. 25, no. 5, pp. 653–663, May 2006.

[6] M. Reyes, G. Malandain, P. Koulibaly, M. Gonzàlez-Ballester, and J. Darcourt, "Model-based respiratory motion compensation for emission tomography image reconstruction," *Phys Med Biol*, vol. 52, pp. 3579–3600, 2007.

[7] G. Wolberg, *Digital image warping*. IEEE Computer Society Press, 1990.

[8] B. De Man and S. Basu, "Distance-driven projection and backprojection in three dimensions," *Phys Med Biol*, vol. 49, no. 11, pp. 2463–2475, 2004.

[9] K. Mueller, R. Yagel, and J. Wheller, "Anti-aliased three-dimensional cone-beam reconstruction of low-contrast objects with algebraic methods," *IEEE Trans Med Imag*, vol. 18, no. 6, pp. 519–537, 1999.

[10] R. Zeng, J. Fessler, and J. Balter, "Estimating 3-D respiratory motion from orbiting views by tomographic image registration," *IEEE Trans Med Imag*, vol. 26, no. 2, pp. 153–163, 2007.

[11] P. Lacroute, "Fast volume rendering using a shear-warp factorization of the viewing transformation," Ph.D. dissertation, Stanford University, 1995. [Online]. Available: http://www-graphics.stanford.edu/papers/lacroute_thesis/

[12] P. Joseph, "Improved algorithm for reprojecting rays through pixel images," *IEEE Trans Med Imag*, vol. MI-1, pp. 192–196, 1982.

[13] A. Lujan, E. Larsen, J. Balter, and R. Ten Haken, "A method for incorporating organ motion due to breathing into 3D dose calculations," *Med Phys*, vol. 26, no. 5, pp. 715–720, 1999.

[14] V. Boldea, D. Sarrut, and S. Clippe, "Lung deformation estimation with non-rigid registration for radiotherapy treatment," in *Medical Image Computing and Computer-Assisted Intervention (MICCAI)*, S. V. L. N. in Computer Science, Ed., vol. 2878, Montréal, Canada, 2003, pp. 770–777.